Plasma Chemistry and Plasma Processing, Vol. 14, No. 3, 1994

Diagnostics of a Thermal Plasma Jet by Optical Emission Spectroscopy and Enthalpy Probe Measurements

W. L. T. Chen,[1] J. Heberlein,[1] and E. Pfender[1]

Received September 6, 1993; revised October 6, 1993

An accurate determination of electron density, temperature, and velocity distributions is of primary interest for the characterization of steady-state thermal plasma spray jets. Our diagnostic capabilities based on optical emission spectroscopy include measurements of absolute emission coefficients and Stark broadening. In addition, enthalpy probe diagnostics has also been used for temperature and velocity measurements. Observation of large discrepancies between temperatures derived from absolute emission coefficients, Stark broadening, and from enthalpy probe measurements indicate that severe deviations from LTE (local thermal equilibrium) exist in various regimes of plasma spray jets. Nonequilibrium characterization of such turbulent thermal plasma jets suggests that diffusion of high-energy electrons into the fringes of plasma jets and deviations from chemical equilibrium due to high velocities in the core of plasma jets and entrainment of cold gas, are the main reasons for these discrepancies. The establishment of a reliable data base, taking these nonequilibrium effects into account, is a prerequisite for meaningful modeling of real plasma jets.

KEY WORDS: Thermal plasma jet; nonequilibrium characterization; optical emission spectroscopy; Stark broadening; enthalpy probe; electron density, temperature and velocity.

1. INTRODUCTION

Accurate determination of electron density, temperature, and velocity distributions in various regimes of the plasma plume is of primary interest for the diagnostics of thermal plasma spray jets. Although it is well known that typical plasma spray jets exhibit strong axial and longitudinal fluctuations, the measurements reported in this paper are time-averaged data.

In a series of our experimental studies,[1-9] optical emission spectroscopy and enthalpy probe diagnostics have been applied for determining temperature, velocity, and electron density fields in turbulent argon–helium plasma

[1]ERC for Plasma-Aided Manufacturing and Department of Mechanical Engineering, University of Minnesota, Minneapolis, Minnesota 55455.

0272-4324/94/0900-0317$07.00/0

jets. Spectrometric methods based on measurements of absolute line and continuum intensities have been used for measuring temperatures above 9000 K.[1] Enthalpy probes have been applied for measuring temperatures between 2000 and 11,000 K.[2] The Stark broadening technique covers a measurement range of electron densities from 2×10^{16} to 2×10^{17} cm^{-3}.[8,9] Water-cooled enthalpy probes have also been applied for the determination of plasma flow velocities by stagnation pressure measurements.[5,6]

Substantial discrepancies between temperatures derived from emission spectroscopy and from enthalpy probes exceeded by far the error limits inherent for both methods.[5,10] The higher values obtained from spectroscopy have been interpreted to be due to deviations from LTE (local thermal equilibrium). This finding led to the suggestion to apply electron density measurements by using Stark broadening, which is independent of the assumption of LTE.[8,9] Strong discrepancies between the electron densities derived from Stark broadening of the H_β line and those from spectrometric and enthalpy probe measurements based on the assumption of LTE pointed to strong nonequilibrium effects in plasma jets.

Departure from LTE is a phenomenon of substantial importance for energy transfer in thermal plasma jets. For diagnosing and defining the nonequilibrium situation in plasma jets, the accuracy and reliability of experimental data must be assured. An analysis of experimental errors and an evaluation of our experimental methods have been performed, and the results will be reported in this paper.

2. EXPERIMENTAL SET-UP AND METHODS

2.1. Plasma Source

A commercial d.c. plasma spray gun (Miller SG-100 with Mach I setting) was used as the plasma generator mounted in a water-cooled chamber with an opening to the atmospheric environment. The torch current was set at 800 A, and the primary and secondary gas for the plasma jet were argon and helium with flow rates of 100 scfh and 47 scfh, respectively. For measuring the spectral line profiles of H_β, hydrogen gas with a flow rate of 3 scfh was added to the Ar/He flow.

2.2. Experimental Set-Up

A schematic diagram of the experimental methods used for diagnosing the nonequilibrium situation in plasma jets is shown in Fig. 1, and a sketch of the experimental set-up is shown in Fig. 2. The set-up consists of an optical and spectrometric arrangement, an optical multichannel analyzer (OMA), an enthalpy probe measurement system, and a host computer. A

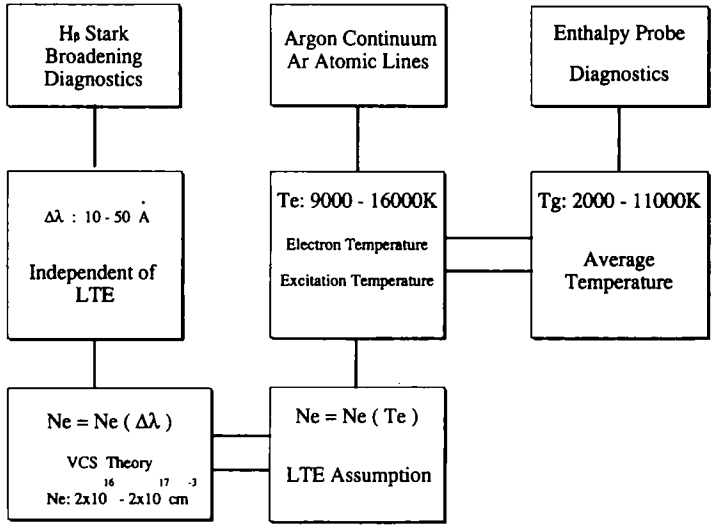

Fig. 1. Diagnostic methods for nonequilibrium situation in plasma jets.

host microcomputer, model IBM PS/2, was interfaced with the measurement systems for automatic control. An IEEE-488 interface board (National Instruments, Model MC-GPIB) was installed in the IBM PS/2 for communication between the microcomputer and the OMA system.

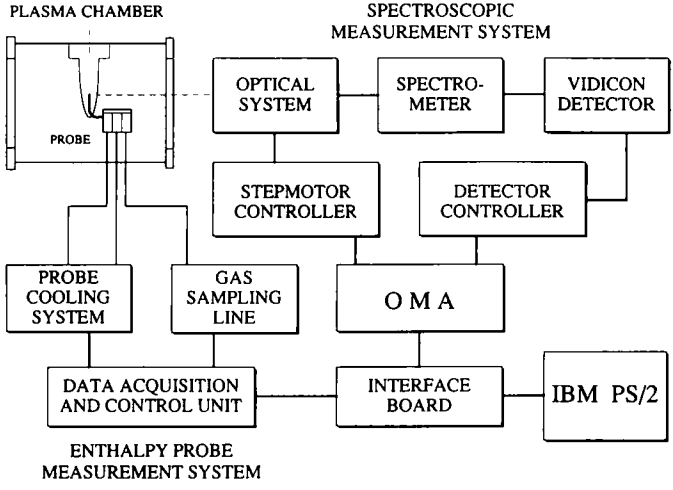

Fig. 2. Schematic of experimental set-up.

An OMA Model 1460-V, EG&G PARC was used to acquire and display the spectral data.[1] A 2 : 1 reduced image of the plasma jet flame in side-on observation is cast on the entrance slit of a spectrometer (model HR320, Instruments SA, Inc, grating 1800 grooves/mm, entrance slit width 0.025 mm, linear dispersion in first order of the grating 18 Å/mm, resolution 0.3 Å). This demagnification of the optical system was kept constant during the scanning procedures. The axial position along the plasma jet was controlled by proper positioning of optical components which are driven by stepping motors which, in turn, were energized by a controller (model Velmex 86 mm-2 interfaced with the OMA 1460-V). The vidicon detector (model 1254 in the OMA system) is turned by 90° and installed in the exit focal plane of the spectrometer. The horizontal scanning of an electron beam in this detector was assigned to the location in the plasma, and the different tracks correspond to the different wavelengths of the plasma radiation. The optical system was precisely aligned with a laser beam.

2.3. Measurements of Absolute Emission Coefficients

The intensities of the argon continuum at a wavelength of 432.1 nm and an atomic spectral line at 430.0 nm were measured for temperature determination based on the assumption of LTE. The spectral intensity calibrations were performed by using a pyrometric MOLARC lamp (model 2371) which has a stable operation at specified experimental conditions.[1] Radial distributions of the absolute emission coefficients of the argon continuum or of an argon atomic line were obtained by the Abel inversion.

2.4. Stark Broadening Technique

Stark broadening of the H_β line was used for electron density determination.[11-18] For a certain vertical position $z = d_n$ from the nozzle exit in the plasma jet ($n = 1$-20, $\Delta d = 2$ mm), the experimental procedure of data acquisition and analysis for H_β Stark broadening measurement was carried out as follows.[8,9]

2.4.1. Intensity Measurements

For obtaining intensity distributions $I(\lambda_m, x, d_n)$ of H_β as a function of the lateral position x within the plasma jet for different wavelengths $\lambda_m (m = -40$ to $+40)$ in side-on observation, the channel scannings in the vidicon detector was assigned to the lateral x position within the jet, and the different 81 tracks correspond to the 81 wavelengths that were screened.

2.4.2. Abel Inversion

Radial distributions $\varepsilon(\lambda_m, r, d_n)$ of the emission coefficient as a function of radius r for different wavelengths $\lambda_m (m = -40$ to $+40)$ were obtained by Abel inversion.

2.4.3. Data Transformation

For obtaining the spectral line shapes $\varepsilon(\lambda, R_k, d_n)$ as a function of wavelength λ for different radii $r = R_k (k = 0\text{–}40)$, the data transformation from $\varepsilon(\lambda_m, r, d_n)$ to $\varepsilon(\lambda, R_k, d_n)$ must be performed.

2.4.4. Half-Width Evaluation (or Best-Fit with Theoretical Shapes of H_β)

The half-width data of H_β, $\Delta\lambda(R_k, d_n)$, at different radii $r = R_k (k = 0\text{–}40)$ were obtained from the spectral line shapes $\varepsilon(\lambda, R_k, d_n)$.

2.4.5. Electron Density Evaluation

The electron density data $n_e(R_k, d_n)$ at different radii $r = R_k (k = 0\text{–}40)$ were determined by the VCS theory.[12]

2.5. Enthalpy Probe Diagnostics

For extending the temperature profiles and isotherms to lower temperature levels, an enthalpy probe method was used. An enthalpy probe is generally considered to be a reliable diagnostic tool in the temperature range from 2000 to 11,000 K.[2] This diagnostic tool allows measurements of composition, temperature, and velocity in plasma jets. The enthalpy probe measurement system includes a water-cooled enthalpy probe, a probe cooling system, a gas sampling line, a probe traversing mechanism, and a data acquisition and control unit. The enthalpy probe, with an outer diameter of 3 mm and a sucking port of 0.68 mm, was made of stainless steel and was designed and built at the University of Minnesota. The cooling water of the probe cooling system was pressurized by a high-pressure helium source. Two thermocouples were located at the coolant channel outlet and inlet for measuring the cooling water temperature increase. The third thermocouple was installed at the end of the gas sucking port of the probe and connected to an electronic icepoint for measuring the gas sample temperature. The values of local enthalpies in the plasma can be derived from an energy balance applied to the cooling water flowing through the probe and the gas sample continually being extracted from the plasma. For determining the external heat transfer to the probe, a "tare" measurement is required. The temperature increases were measured, respectively, with sample gas flow and

without sample gas flow from the plasma through the probe. The "tare" measurements (no flow) are controlled by two electro-valves connected to the data acquistion unit model HP3421A. A sonic orifice was adjusted to the critical condition for a gas sample flow around 10 mg/s. The experimental data were averaged for 10 measurements. Before starting the data acquisition, the geometric center of the plasma jet was found by using a laser beam and a corresponding optical system. Then the actual center position of the plasma jet was determined by measuring the stagnation pressures while traversing the probe along two horizontal directions. Data acquisition was entirely computer-controlled. For conversion of enthalpies into temperatures, or stagnation pressures into velocities, knowledge of the thermodynamic state of the plasma is required, which is based on modeling work in this laboratory.[2]

3. NON-EQUILIBRIUM CHARACTERIZATION IN TURBULENT Ar/He PLASMA JETS

Measurements of plasma parameters (including temperatures, velocity, and electron density fields) indicate strong deviations from LTE in Ar/He plasma jets. Based on previous results, the nonequilibrium situation in Ar/He plasma jets is summarized in Table I where T_{spec} is the temperature derived from spectrometric measurements (absolute emission coefficients of argon atomic line at 430.0 nm and argon continuum at 431.2 nm), T_{probe} is the temperature derived from enthalpy probe measurements, $n_e(\Delta\lambda_{Stark})$ is the electron density derived from H_β Stark broadening, $n_e(T_{spec})$ is the electron density derived from spectrometric data and the Saha equation under the assumption of LTE, and $n_e(T_{probe})$ is the electron density derived from enthalpy probe data and the Saha equation assuming LTE. Three regimes in terms of spatial location and mechanism for deviation from LTE were identified. In the laminar regime ($d < 20$ mm), isotherms are parallel to each other, as shown in Fig. 3. Here the plasma jet has a bright and stable core. In the turbulent regime ($d > 50$ mm), the isotherms and velocity isocontours spread out, demonstrating the turbulent characteristics of Ar/He plasma jets (see Fig. 3). Between laminar and turbulent regimes, there is a transition regime in which detailed measurements and analysis were conducted by using three different diagnostic methods.

3.1. Experimental Results

3.1.1. Temperature Measurements

The temperature profiles from emission spectroscopy and those from enthalpy probe data for Ar/He plasma jets are shown in Fig. 4. Comparisons

Table I. Nonequilibrium Characterization in Turbulent Ar/He Plasma Jets

Regime	Location	Temperature	Shape of isotherms	Electron density	Departure from LTE	Dominant physical effects
Laminar regime	$d = 2$ mm, $R = 0$ $d < 20$ mm	$T_{spec} > T_{probe}$	Parallel to jet axis	$n_e(\Delta\lambda_{Stark}) = n_e(T_{spec})$ $n_e(\Delta\lambda_{Stark}) > n_e(T_{spec})$	LTE non-LTE	Electron diffusion, overpopulation of excited states
Laminar-turbulent transition regime	$d = 30$ mm	$T_{spec} > T_{probe}$ $R = 0$, $(\Delta T/T) \sim 20\%$		$n_e(\Delta\lambda_{Stark}) > n_e(T_{spec}) > n_e(T_{probe})$ $R = 0$, $(\Delta n_e/n_e) \sim 100\%$	non-LTE	Chemically frozen flow
Fully turbulent regime	$d > 50$ mm	$T_{spec} > T_{probe}$	Spread out from jet axis		non-LTE	Cold gas entrainment

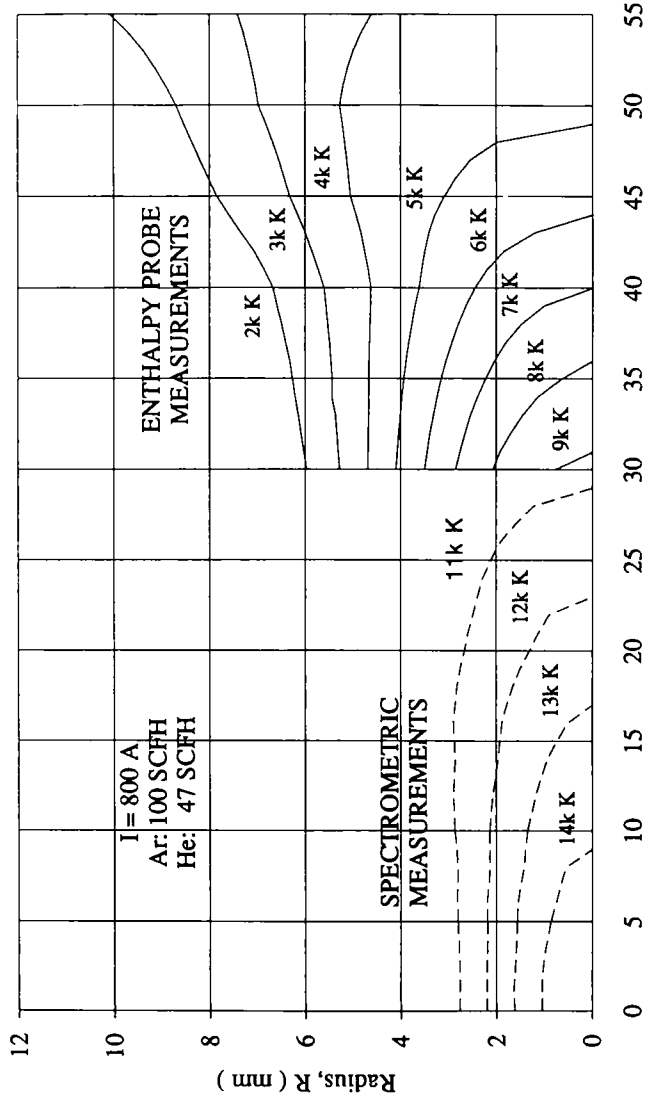

Fig. 3. Isotherms in Ar/He plasma jets.

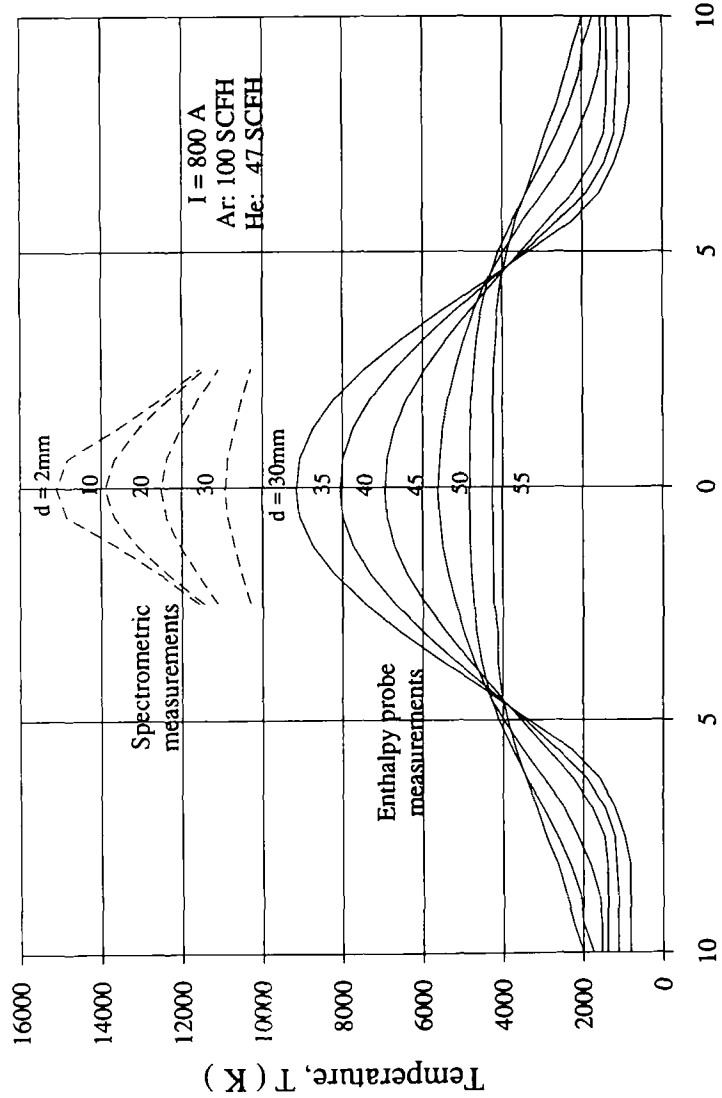

Fig. 4. Temperature profiles derived from emission spectroscopy and from enthalpy probe measurements.

of these data show strong discrepancies between the temperatures derived from the two methods. These discrepancies in various regimes of the plasma jets exceed by far the error limits inherent to both methods. For distances $d < 40$ mm from the anode nozzle, errors involved in enthalpy probe measurements are less than 5%, and the spectrometric measurements have even lower error limits of about 3% for our experimental conditions.[2] Therefore, higher values of temperatures derived from emission spectroscopy are interpreted to be due to deviations from LTE in various regimes of Ar/He plasma jets.

Deviations from LTE in Ar/He jets occur not only in the fringes but also in the center part. In the core of the jet at $d = 30$ mm, the temperature deviation may be as high as 20%. Much stronger deviations occur in the jet fringes.

3.1.2. Electron Density Measurements and Calculations

The Stark broadening method does not require any assumptions about the thermodynamic state of the plasma, because the spectral line broadening is only related to the interaction effects between emitter (atoms) and perturbers (electrons and ions) in the plasma. Since Stark broadening does not require the assumption of LTE, comparisons of electron density data derived from Stark broadening with those derived from other diagnostic methods under the assumption of LTE (simply called "LTE methods") will provide an indication of nonequilibrium effects in the plasma.

Differences between electron density data derived from Stark broadening and LTE methods in various regimes of plasma jets may be identified if the uncertainties of electron density data derived from Stark broadening measurements are much less than the discrepancies between Stark broadening and LTE measurements. The total uncertainty for determining the electron density from Stark broadening in the axial region is ±5%, which includes intensity measurement errors of ±2%, an uncertainty of ±2% caused by the Abel inversion, and uncertainty of ±1% introduced by the data analysis procedures. In the jet fringes, intensity measurements and Abel inversion introduce higher relative errors. When a set of neutral filters was used for intensity measurements, the accuracy of electron density data in the fringe regions was substantially improved, and the total uncertainty was kept below ±10%. Some of the results of electron density distributions are summarized in Fig. 5. The electron densities derived from Stark broadening and those derived from LTE temperatures (dashed lines) are plotted on the right side of Fig. 5, and the corresponding LTE temperatures are plotted on the left half of this diagram. In the axis near the nozzle exit ($d = 2$ mm), the electron density ($n_e = 1.57 \times 10^{17}$ cm^{-3}) derived from Stark broadening

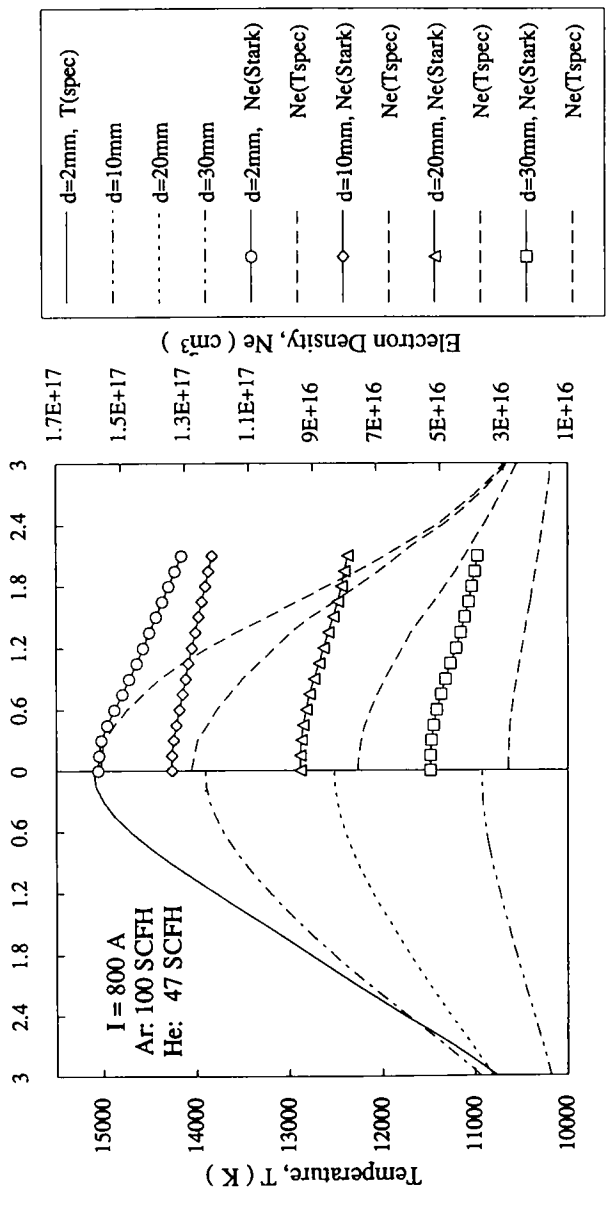

Fig. 5. Comparisons of electron density distributions derived from Stark broadening with those derived from spectrometric temperatures under the assumption of LTE.

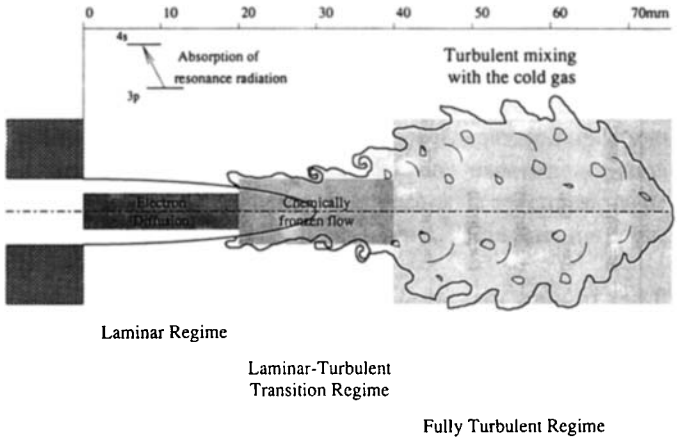

Fig. 6. Nonequilibrium characters in Ar/He plasma jet.

measurements is in good agreement with the value ($n_e = 1.56 \times 10^{17}$ cm^{-3}) derived from spectrometric temperatures with the assumption of LTE. However, the discrepancies between the two types of measurements increase with increasing radial and axial distance from the nozzle exit of the plasma torch. The deviations become as high as 100% at a radial distance of $r = 2$ mm. These results indicate that substantial deviations from LTE occur in various regimes of the jet plume except in the region very close to the jet axis near the nozzle exit where LTE seem to exist.

3.2. Dominant Physical Effects Causing Deviations from LTE

Different physical effects may be responsible for deviations from LTE in various regimes of Ar/He plasma jets, as indicated in Table I. A schematic of a thermal plasma jet based on the results of Table I is shown in Fig. 6.

3.2.1. Diffusion Effects

As the plasma jet exits the anode nozzle, it encounters steep radial gradients in the fringes. The jet appears to have a stable laminar core, as suggested by the parallel isotherms up to around $d \sim 20$ mm (Fig. 3). The steep radial gradients of electron densities in the region very close to the nozzle exit (up to $dn_e/dr = 1.6 \times 10^{17}$ cm^{-4}) induce diffusion of high-energy electrons from the core towards the jet fringes. Therefore, true electron densities derived from Stark broadening are substantially higher than those derived from other spectrometric measurements, and the discrepancies increase with increasing radial distance from the jet axis. Collisional

excitations[9] of high-energy electrons in the fringes will cause higher population densities of the excited states of the argon atoms. Consequently, these higher populations will lead to an overestimation of temperatures derived from line or continuum intensities.

Another possible mechanism which may contribute to the higher population densities of excited states in the fringes of plasma jets may be absorption of resonance radiation by argon atoms. Resonance radiation emitted from the hot core of the plasma jet may be reabsorbed over relatively short distances by argon atoms in the jet fringes which are essentially in the ground state.[19] Fincke *et al.*[19] concluded that the large differences in the measured heavy-particle kinetic temperatures from laser scattering and from emission spectroscopy are due to reabsorption of resonance radiation. In contrast, our results suggest that electron diffusion is the primary source for such deviations in regimes of high electron density gradients.

In addition, sources of nonequilibrium in thermal argon plasmas have also been investigated and analyzed in recent studies of a free-burning argon arc.[20] Farmer and Haddad[20] found that a considerable discrepancy exists between the number densities of argon atoms derived from Rayleigh scattering and those obtained from argon line emission in the outer regions of argon arcs where the temperatures are below 8000 K and electron densities are below $10^{15}\,\mathrm{cm}^{-3}$. Cram *et al.*[21] proposed a magnetogasdynamic arc model combined with a collisional-radiative model to explain those kinds of discrepancies. They concluded that this nonequilibrium situation is caused by intense resonance line radiation from the arc core absorbed in the arc fringes leading to an overpopulation of the excited argon atoms with respect to the ground state. As previously mentioned, this situation of reabsorption of resonance radiation may also occur in the outer fringes of argon/helium plasma jets ($r > 2$ mm and $d > 30$ mm) where electron densities drop below $10^{16}\,\mathrm{cm}^{-3}$ and temperatures below 9000 K. Electron diffusion, however, will be important around the jet center ($r < 2$ mm) where electron densities exceed $10^{16}\,\mathrm{cm}^{-3}$ and temperatures exceed 10,000 K.

Besides electron diffusion, diffusion of heavy species and the associated demixing effects in Ar/He plasmas have to be considered. A calculation[4,7] has qualitatively confirmed the diffusion effects of argon and helium atoms. Based on the existence of LTE in the region very close to the jet axis near the nozzle exit, the equilibrium compositions with diffusion effects for the Ar/He mixture have been calculated. The results indicate that a significant demixing effect occurs, i.e., the population of He atoms in the center of the jet ($T_{\mathrm{center}} \sim 15{,}000$ K) due to diffusion is substantially higher than the corresponding equilibrium value. In contrast, diffusion exerts only a small effect on the concentration of argon atoms in this regime. The reason is that argon and helium gases have different ionization potentials. While electrons

and ions diffuse toward the fringes, both argon and helium atoms diffuse toward the center. Under the specified temperature condition of $T_{center} \sim 15{,}000$ K, the concentration of helium atoms near the center increases almost entirely due to diffusion, because ionization of helium can be neglected. The concentration of argon atoms near the center would increase due to diffusion of argon atoms from the fringes, but depletion of argon atoms due to ionization overcompensates this effect. The argon concentration shows only a minor deviation for cases with or without diffusion. The concentration of argon atoms follows essentially the equilibrium distribution. Therefore, for spectrometric measurements in this regime, argon lines should be used unless diffusional effects are taken into account.

3.2.2. Chemically Frozen Flow Effect

At the jet centerline near the nozzle exit, the velocity of the plasma flow exceeds 1000 m/s.[8,19] Due to this high jet velocity, the travel time of plasma volume element from the nozzle exit to a location $d \sim 30$ mm downstream is of the same order of magnitude as the relaxation time (~ 10 μs).[19] Therefore, a chemically frozen flow situation may be approached up to a distance of $d = 30$ mm, which is located between the laminar and the fully turbulent regimes. This partially frozen chemistry will maintain higher electron densities in this regime, i.e., the electron density derived from Stark broadening at $d = 30$ mm ($n_e = 5.3 \times 10^{16}$ cm^{-3}) will be substantially higher than that derived from LTE temperatures. The discrepancy of electron densities between the two methods may be as high as 100% in the laminar–turbulent transition regime. It should be pointed out that the chemically frozen flow conditions may be favorable for enhancing heat transfer to the spray powders.

The higher electron densities due to frozen flow effects will lead to higher population densities of excited states by electron-atom collisions. This, in turn, will give rise to higher temperatures derived from emission spectroscopy. Enthalpy probe measurements will be little affected by the higher population densities of excited states, because their contribution to the enthalpy is negligible. Therefore, it is not surprising that enthalpy probe measurements result in temperatures up to 20% lower (at $d = 30$ mm on the axis of the plasma jet) than those derived from emission spectroscopy.

In following the regime, the section farther downstream ($d > 30$ mm) will be considered, which is governed by entrainment of cold gas.

3.2.3. Cold Gas Entrainment Effect

The engulfment of cold gas eddies into the plasma plume in the transitional and fully turbulent regime results in strong discrepancies between spectrometric temperatures and enthalpy probe data. Obviously, spectro-

metric measurements record only radiation from the high-temperature plasma and disregard the cold gas entrained into the plasma plume, whereas enthalpy probes measure average temperatures resulting from both hot and cold gas.

As shown in previous studies,[3,10] the entrained gas "bubbles" behave in a first approximation as solid particles, causing a rapid reduction of the jet velocity. As the entrained gas "bubbles," accelerated by the surrounding plasma flow, gradually dissolve by convection and molecular diffusion, the temperature of the mixture is substantially reduced. Both Stark broadening and emission spectroscopy are no longer feasible in this regime because of low electron densities ($< 10^{16}$ cm^{-3}) and low temperatures (< 9000 K). Enthalpy probes, however, are a relatively inexpensive and simple tool for both enthalpy (temperature) and velocity measurements in this regime. Limitations on spatial resolution and flow disturbance, which are inherent disadvantages of probe measurements, must be taken into account.

4. CONCLUSIONS

Understanding of nonequilibrium situations in Ar/He plasma jets has been greatly enhanced by using optical emission spectroscopy, Stark broadening, and enthalpy probe diagnostics.

Precise measurements and error analysis have been performed for ascertaining the accuracy and reliability of electron density data from Stark broadening. The discrepancies between Stark broadening and LTE methods exceed by far the error limits inherent to those methods. The errors for electron density measurements involved in the Stark broadening technique are less than 5% in the axis and less than 10% in the fringes of plasma jets. The errors involved in enthalpy probe measurements are less than 5%, and the absolute emission coefficient measurements have even lower errors of about 3%. Comparisons of temperatures or electron densities derived from different diagnostic methods clearly demonstrate that severe deviations from LTE occur in various regimes of turbulent Ar/He plasma jets. Diffusion of high-energy electrons into the jet fringes, partially frozen chemistry, and cold gas entrainment may be the dominant physical effects causing departures from LTE in the laminar, laminar–turbulent transition, and fully turbulent regime, respectively.

Application of optical emission spectroscopy will result in erroneous data for temperature measurements if LTE is assumed, with the exception of a small region close to the nozzle exit. Stark broadening provides reliable data for electron densities in regimes of high electron densities ($\geq 10^{16}$ cm^{-3}). The enthalpy probe method is a reliable and meaningful diagnostic tool for investigating plasma properties in plasma spray jets, particularly for those

plasma plume areas in which other methods are no longer valid. The possible effects which fluctuations of the plasma jet may have on the reported data have not been included in this study.

ACKNOWLEDGMENTS

This work was supported by NSF/CDR-87-21545. The U.S. Government has certain rights in this material.

REFERENCES

1. W. L. T. Chen and E. Pfender, *Proc. of 9th International Symposium on Plasma Chemistry,* Pugnochiuso, Italy (1989), p. 330.
2. W. L. T. Chen and E. Pfender, Enthalpy probe and spectroscopic measurements in thermal plasma jets, *Report, ERC for Plasma-Aided Manufacturing*, Department of Mechanical Engineering, University of Minnesota (1990).
3. E. Pfender, W. L. T. Chen, and R. Spores, *Proc. of 1990 National Thermal Spray Conference,* Long Beach, California (1990), p. 1.
4. E. Pfender, W. L. T. Chen, C.-P. Chiu, and J. Heberlein, *Studies of a Turbulent Argon–Helium Plasma Jet*, 1991 National Thermal Spray Conference, Pittsburgh, Pennsylvania (1991).
5. W. L. T. Chen, J. Heberlein, and E. Pfender, *Proc. of 10th International Symposium on Plasma Chemistry,* Bochum, Germany, 1.2–12 (1991).
6. W. L. T. Chen, J. Heberlein, and E. Pfender, *Experimental Measurements of Plasma Properties for Miller SG-100 Torch with Mach I Setting,* Idaho National Engineering Laboratory Report, EGG-SCM-9576, EG&G Idaho, Inc., Idaho Falls, Idaho (1991).
7. E. Pfender, W. L. T. Chen, C.-P. Chiu, and J. Heberlein, *Properties of a Turbulent Argon–Helium Plasma Jet*, Werkstofftechnologie in Wandel, H. Kern, ed., Deutscher Verlag für Schweisstechnik, Düsseldorf, Germany (1991), p. 71.
8. W. L. T. Chen, J. Heberlein, and E. Pfender, *Proc. of Symposium on Thermal Plasma Applications in Materials and Metallurgical Processing*, TMS Annual Meeting, San Diego, California (1992), p. 107.
9. W. L. T. Chen, J. Heberlein, and E. Pfender, *Proc. of 1992 International Thermal Spray Conference,* Orlando, Florida (1992), p. 327.
10. E. Pfender, J. Fincke, and R. Spores, *Plasma Chem. Plasma Process.* **11**, 529 (1991).
11. P. Kepple and H. R. Griem, *Phys. Rev.* **173**, 317 (1968).
12. C. R. Vital, J. Cooper, and E. W. Smith, *J. Quant. Spectrosc. Radiat. Transfer* **11**, 263 (1970).
13. W. L. Wiese, D. E. Kelleher, and D. R. Paquette, *Phys. Rev. A* **6**, 1132 (1972).
14. R. C. Preston, *J. Quant. Spectrosc. Radiat. Transfer* **18**, 337 (1977).
15. P. Baessler and M. Kock, *J. Phys. B* **13**, 1351 (1980).
16. A. Scheeling, J. P. Kamla, and M. J. Zoellner, *Spectrochim. Acta* **39B**, 677 (1984).
17. E. H. Choot and G. Horlick, *Spectrochim. Acta* **41B**, 935 (1986).
18. C. Thomson and U. Helbig, *Spectrochim. Acta* **46B**, 1215 (1991).
19. J. R. Fincke, T. J. Repetti, S. C. Snyder, G. D. Lassahn, and B. A. Detering, *Proc. of Symposium on Thermal Plasma Applications in Materials and Metallurgical Processing*, TMS Annual Meeting, San Diego, California (1992), p. 85.
20. A. J. D. Farmer and G. N. Haddad, *J. Phys. D: Appl. Phys.* **21**, 426 (1988).
21. L. E. Cram, L. Poladian, and G. Roumeliotis, *J. Phys. D: Appl. Phys.* **21**, 418 (1988).